Hindawi
International Journal of Corrosion
Volume 2018, Article ID 5250713, 11 pages
https://doi.org/10.1155/2018/5250713

Research Article

Metal Matrix Composite Coatings of Cupronickel Embedded with Nanoplatelets for Improved Corrosion Resistant Properties

Casey R. Thurber,[1] **Yahia H. Ahmad**,[2] **Margaret C. Calhoun**,[1] **Amaal Al-Shenawa**,[3] **Nandika D'Souza**,[3] **Adel M. A. Mohamed**,[2] **and Teresa D. Golden**[1]

[1]*Department of Chemistry, University of North Texas, Denton, TX 76203, USA*
[2]*Department of Metallurgical and Materials Engineering, Faculty of Petroleum and Mining Engineering, Suez University, Suez 43721, Egypt*
[3]*Department of Mechanical and Energy Engineering, University of North Texas, Denton, TX 76207, USA*

Correspondence should be addressed to Teresa D. Golden; tgolden@unt.edu

Received 24 January 2018; Accepted 17 April 2018; Published 3 June 2018

Academic Editor: Phuong Nguyen-Tri

The deterioration of metals under the influence of corrosion is a costly problem faced by many industries. Therefore, particle-reinforced composite coatings are being developed in different technological fields with high demands for corrosion resistance. This work studies the effects of nanoplatelet reinforcement on the durability, corrosion resistance, and mechanical properties of copper-nickel coatings. A 90 : 10 Cu-Ni alloy was coelectrodeposited with nanoplatelets of montmorillonite (Mt) embedded into the metallic matrix from electrolytic baths containing 0.05, 0.10, and 0.15% Mt. X-ray diffraction of the coatings indicated no disruption of the crystal structure with addition of the nanoplatelets into the alloy. The mechanical properties of the coatings improved with a 17% increase in hardness and an 85% increase in shear adhesion strength with nanoplatelet incorporation. The measured polarization resistance increased from 11.77 $k\Omega \cdot cm^2$ for pure Cu-Ni to 33.28 $k\Omega \cdot cm^2$ for the Cu-Ni-0.15% Mt coating after soaking in a simulated seawater environment for 30 days. The incorporation of montmorillonite also stabilized the corrosion potential during the immersion study and increased resistance to corrosion.

1. Introduction

Introduction of nanofillers and nanocrystalline phases into functional coatings can enhance the performance and properties of the nanocomposite coatings [1–3]. For example, metal matrix composite (MMC) coatings that slow the rate of corrosion at a reduced cost are an important area of study [4–7]. The MMC coatings can be produced by various techniques such as hot pressing, stir casting, diffusion bonding, powder metallurgy, and chemical vapor deposition [8]. However, some drawbacks to these methods include production at high temperatures or under vacuum, difficulty in controlling the thickness, and cost. As the accessibility of nanoparticles continues to rise, the interest in reduced cost and low temperature deposition of MMCs continues to increase [9].

Electrodeposition is an interesting method for producing new materials, especially in the field of MMCs. The electrodeposition technique has several advantages over other processing methods which include low cost, simplicity of operation, versatility, high production rates, industrial applicability, control of film thickness, and few size and shape limitations [9]. Electrodeposited composites are of particular interest because of their unique and often superior properties compared with their counterparts. The electrodeposition of a metal matrix composite involves the electrolysis of the plating bath where nanosized particles are dispersed and various amounts of the particles become embedded within the plated metal matrix producing a reinforced composite [10, 11]. Successful incorporation of nanoparticles into the metal matrix by electrocodeposition relies on several parameters, including composition of the electrolyte, pH, current density, and properties of the particles [12]. By systematic control of these parameters, microstructure and property performance can be optimized for the composites. Researchers have used

electrochemical deposition to improve corrosion resistant properties of various alloys with addition of nanoparticles such as In_2O_3, [13], SiC, [14, 15], Al_2O_3, [16], and TiO_2, [17]. Also, multilayer coatings and functionally graded nanocomposite coatings can be produced using a pulse electrodeposition technique. The addition of a second phase, such as Al_2O_3 into Ni-Fe alloys, can improve wear properties and microhardness of these coatings [18–20]. Ni-W coatings, which have good wear and corrosion properties but are prone to cracking, can be significantly improved by using electrodeposition to produce a functionally graded nanocomposite coating containing Al_2O_3 [21, 22]. The coating is deposited so that the alumina content increases towards the surface and exhibits increase in corrosion resistance compared to the pure alloy or metal coating.

Cu-Ni alloys have many different uses including coatings for pipeline in marine environments, condensers, microelectronics, and heat exchangers [23–25]. Copper-nickel alloys are used extensively in multistage flash (MSF) and multiple effect distillation (MED) plants since they have high corrosion resistance under high chloride and temperature conditions commonly encountered in the desalination process [26, 27]. Copper alloys are used in marine environments to defend against biofouling by inhibiting microbial induced corrosion (MIC) [28]. The two most common copper alloys are 90-10 Cu-Ni (90% Cu and 10% Ni, Alloy 70600) and 70-30 Cu-Ni (70% Cu and 30% Ni, Alloy C71500) [29]. 90-10 Cu-Ni coatings produce better protection in more stagnant conditions, whereas the 70-30 Cu-Ni coatings are used in higher flow conditions because of the increased hardness provided by the higher concentration of nickel [29]. The 90-10 Cu-Ni alloy has a good balance of properties and is more cost effective than the 70-30 composition, which makes it popular for several applications [29]. 90-10 Cu-Ni has been studied in long term quiescent environmental exposure and it was found that the corrosion rate dropped below 2.5 μm/year after the protective oxide layer was fully formed versus 10.1 μm/year for the 70-30 Cu-Ni alloy [28]. When the concentration of nickel is below 40%, an outer layer of $Cu_2(OH)_3Cl$ and a dense inner layer of Cu_2O form a passivating layer in high chloride environments [30]. Different ions such as nickel and iron can be incorporated into the Cu_2O layer because of the presence of vacancies [30–33]. Once the Cu_2O layer has formed, the $Cu_2(OH)_3Cl$ layer is produced by precipitation from the dissolution of Cu^{2+} ions [30, 32].

The addition of ceramic nanoparticles, such as nanoplatelets, can enhance the durability and therefore the lifetime of the alloy coatings [34, 35]. Montmorillonite (Mt), a clay mineral, has a layered structure with a thickness in the nanometer range and plate-like stacking structure. Mt possesses several desired properties including high specific surface area, cation exchange capacity, resistance to a wide range of temperatures, pH resistance, and chemical inertness. Once the platelets are embedded into the metal matrix, the overall thermal stability and mechanical strength of the coating increase [36]. The incorporated Mt embedded into a pure nickel matrix has led to enhanced adhesion, hardness, and corrosion resistance [36, 37]. Relatively few studies exist on the electrodeposition of copper-nickel composites and majority of the work has focused on applications for MEMS devices or mechanical properties [38–40]. Previous work on 70-30 Cu-Ni composites reported an increase in the corrosion resistance and mechanical properties [41]. The aim of the present work is to study and evaluate the corrosion behavior and mechanical properties of electrodeposited 90-10 Cu-Ni composite coatings reinforced with Mt. The 90-10 Cu-Ni ratio is advantageous in some environmental extreme conditions and offers a lower cost alternative compared to other alloys. The resulting corrosion products on the surface of the coatings after 30 days are studied and compared to Cu-Ni pipe surfaces.

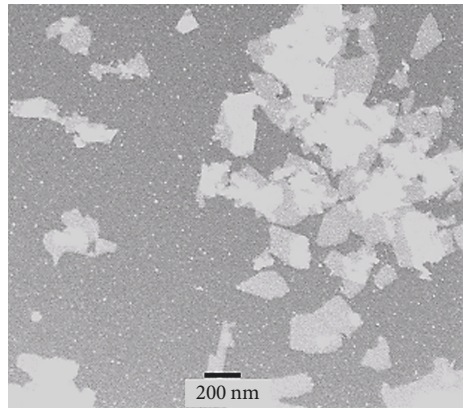

Figure 1: TEM image of exfoliated pure Na-montmorillonite after mechanically stirring in deionized (DI) water for 24–48 hours to break apart the stacking of the nanoplatelets.

2. Experimental Procedure

2.1. Materials. The chemicals used in the plating baths were $Ni(NH_4)_2(SO_4)_2{\cdot}6H_2O$ (Alfa-Aesar), $NiSO_4{\cdot}6H_2O$ (Fisher), $Na_3C_6H_5O_7{\cdot}6H_2O$ (Fisher), $H_3C_6H_5O_7$ (Fisher), $CuSO_4{\cdot}5H_2O$ (Fisher), Na-montmorillonite (Mt) (Southern Clay Products), and NaOH (Fisher). Mt is a clay mineral, which has the formula (Na, Ca) $(Al_{1.66}\ Mg_{0.33})_3\ (Si_4O_{10})_3\ (OH)_6{\cdot}n(H_2O)$. The individual Mt platelets are ~1-2 μm in length and 1 nm in height [42]. Since clay mineral contains layers stacked on top of each other, the Mt had to first be exfoliated before the deposition process. Therefore, the Mt was vigorously mechanically stirred in deionized (DI) water for 24–48 hours to break apart the stacking of the nanoplatelets. Figure 1 shows the TEM image of the Mt where the individual platelets can be seen after exfoliation. Citrate was used as the ligand in the electrochemical baths containing copper and nickel ions since citrate complexes with the metal ions [43–45]. The working, counter, and reference electrodes were a stainless steel substrate, coiled chromel wire, and a saturated calomel reference (SCE), respectively. Stainless steel (Grade 430) substrates (area of 1.768 cm^2) were used as the working electrodes and mechanically polished with different grade emery papers followed by a sequence of cleanings (sonication in ethanol/deionized water) to prepare the substrate surface for electrodeposition. The substrates

Table 1: Deposition conditions for the Cu-Ni-Mt composite coatings.

$Ni(NH_4)_2(SO_4)_2{\cdot}6H_2O$	0.24 M
$CuSO_4{\cdot}5H_2O$	0.06 M
$Na_3C_6H_5O_7{\cdot}2H_2O$	0.25 M
Montmorillonite (Mt)	0–0.15%
Applied voltage	−1.0 V
Charge	30 C
Temperature	25°C
pH	6.0

were then activated by dipping in a 5.0 M H_2SO_4 solution for about 3–5 minutes.

2.2. Electrodeposition Procedure. An EG&G Princeton Applied Research Model 273A potentiostat/galvanostat was used for the electrodeposition of the coatings. The electrochemical bath conditions are listed in Table 1. To adjust the pH of the electrochemical bath to 6, a 6.0 M NaOH solution was used. The solution was purged with N_2 for 15 minutes to deaerate the electrochemical bath before deposition. The stainless steel electrodes were coated with a thin seed layer of nickel first to obtain good adhesion for the Cu-Ni coatings onto the substrate [43]. A pH 2.5 buffered nickel-citrate electrochemical bath was used to deposit the thin seed layer (1.5 Coulombs), which contained 77.8 g/L $NiSO_4{\cdot}6H_2O$, 35.3 g/L $Na_3C_6H_5O_7{\cdot}6H_2O$, and 34.6 g/L $H_3C_6H_5O_7$ [46]. After electrodeposition, the composite coating was rinsed with deionized water.

2.3. Characterization Techniques. The minimum adhesion of the coatings was measured with a DeFelsko, PosiTest AT-A (automatic) Pull-Off Adhesion Tester. All the coatings were found to have adhesion values greater than 75 N/mm^2; this indicated that the coatings were intact and showed no signs of peeling or flaking off the surface. The film thickness for the coatings was measured using a Veeco Dektak 8 Stylus Profilometer.

The zeta potential and particle size of the Cu-Ni plating solutions were measured using a Delsa Nano-C (Beckman-Coulter Instruments) to determine the stability of Mt in the Cu-Ni plating bath. The Cu-Ni solutions were allowed to equilibrate at 25°C for 90 seconds using a Peltier device in the instrument before data collection.

Atomic absorption spectroscopy (AAS) (Perkin Elmer Analyst 300) was used to determine the Cu and Ni percentages in the electrodeposited coatings. The coatings were soaked and dissolved first in 50/50 DI H_2O/HNO_3 solution before aspiration into the AAS. The standard addition method was used to determine the optimal metal concentrations for the plating bath in order to obtain a 90-10 Cu-Ni ratio.

X-ray diffraction (XRD) (Siemens D-500 Diffractometer) was performed to elucidate the crystal structure and particle size of the Cu-Ni composite coatings. The scans were performed using a Cu Kα radiation source λ = 0.15406 nm at 35 kV and 24 mA. Typical scans were obtained from 40–100° 2θ at a 0.05° step size and a 1-second dwell time. XRD was performed from 10–80° at a 0.05° step size and a 1-second dwell time to determine the corrosion products present at the surface of the composite coatings after being submersed in a simulated seawater for 30 days. Scanning Electron Microscopy (SEM) was used to determine the surface morphology of the composite coatings. FEI Quanta 200 field-emission gun environmental scanning electron microscope coupled with energy dispersion spectroscopy (EDS) was used to determine the elemental composition of Cu-Ni and the Mt (Al and Si) on the composite coatings surface.

A Buehler microhardness instrument model Micromet 5101 (Mitutoyo Corp., Japan) was used to determine the effect of Mt incorporation on the hardness of the Cu-Ni matrix composites. The applied load was 10 gf for 20 s. The final value for the hardness of the coatings was the average of 10 measurements. Shear adhesion tests were measured using the XYZTEC instrument paired with a 2 mm wide knife. The knife was placed at 5 μm above the substrate-coating interface and moved 2 mm horizontally at a velocity 150 μm/s without hold time. The force to move as a function of distance was noted. The adhesive strength is the maximum recorded force divided by the area width of the knife × test distance.

An EG&G Princeton Applied Research Model 273A potentiostat/galvanostat was used for the cyclic voltammetry (CV) and immersion test. Corrosion tests and the open circuit potential (OCP) study for the Cu-Ni and Cu-Ni-Mt coatings were conducted for 30 days in a simulated seawater bath using the composition prescribed by Burkholder's Formula B [24, 47] (per liter of deionized water): 23.476 g NaCl; 3.917 g Na_2SO_4; 0.192 g $NaHCO_3$; 0.664 g KCl; 0.096 g KBr; 10.61 g $MgCl_2$ $6H_2O$; 1.469 g $CaCl_2$ $2H_2O$; 0.026 g H_3BO_3; 0.04 g $SrCl_2$ $6H_2O$. Potentiodynamic polarization was performed on a Parstat 4000 (Princeton Applied Research) running Versa Studio software. A three-electrode electrochemical cell was used as the corrosion testing system which was comprised of the working electrode coatings, two counter graphite rods, and a saturated calomel electrode (SCE) as the reference electrode. Potentiodynamic polarization was performed at a ±250 mV potential range and a scan rate of 0.1667 mV/s. The i_{corr} value was calculated using the Stern-Geary equation, where β_a and β_c are the respective anodic and cathodic Tafel slopes. Linear polarization was also performed from ±20 mV at 0.1667 mV/s to determine the polarization resistance, R_p, of the composite coatings.

3. Results and Discussion

3.1. Cyclic Voltammetry. Cyclic voltammetry was performed to determine the effect of the Mt on the reduction potential and cathodic current for the Cu-Ni deposition. Since Mt is a nonelectroactive particle, it does not possess a redox couple for the electrodeposition cycle. The cyclic voltammograms in Figure 2 show that no shift was detected in the reduction potential of copper (−0.45 V) or in the peak current, i_{pc}, with the addition of 0.05 to 0.15% Mt into the plating bath. The reduction potential for nickel was not observed because of the onset of hydrogen evolution. It has been noted that the

Table 2: Particle size and zeta potential for Mt solutions and 90-10 Cu-Ni-Mt plating solutions.

Solutions	Particle size (nm) ($n = 3$)	Zeta potential (mV) ($n = 3$)
0.05% Mt	430 ± 20	−39.6 ± 0.4
0.10% Mt	495 ± 15	−39.9 ± 0.3
0.15% Mt	525 ± 20	−39.1 ± 0.5
Cu-Ni-0.05% Mt	2710 ± 90	−20.1 ± 0.5
Cu-Ni-0.10% Mt	3030 ± 70	−19.7 ± 0.4
Cu-Ni-0.15% Mt	3280 ± 80	−19.4 ± 0.4

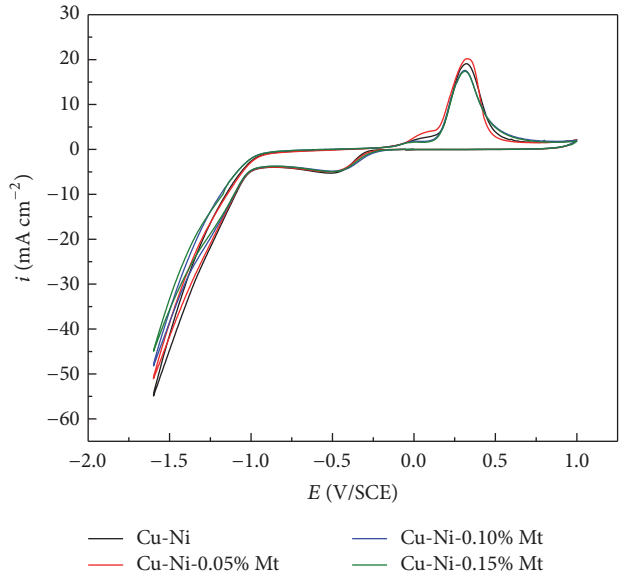

Figure 2: Cyclic voltammograms of the 90-10 Cu-Ni and Cu-Ni-Mt plating solutions, run at a scan rate of 50 mV/s.

concentration of copper in the coating depends on the value of the applied potential. As the voltage increases from −1.0 to −1.075 V, the copper concentration begins to decrease in the film since the deposition of copper is diffusion controlled and the deposition of nickel is charge-transfer controlled [48]. With the addition of Mt into the electroplating solution, the voltammograms showed that the Mt platelets do not affect the redox potentials, but the inclusion of the Mt does help to slightly shift the onset of hydrogen evolution to more cathodic potentials. Therefore, the Mt can be added to the plating bath with no adverse effects on the deposition of the alloy.

3.2. Particle Size and Zeta Potential. Montmorillonite stacked platelets tend to swell when placed in an aqueous environment and starts to mechanically shear apart after vigorous stirring for 24–48 hours. The negatively charged platelets become countered by positively charged copper and nickel ions in the plating solution. During the deposition process, the platelets are thought to be electrostatically attracted to the substrate. The long planar shape of the platelet helps to yield a snug contact with the oppositely charged substrate [42]. The copper and nickel ions are reduced onto the substrate trapping the platelets in the alloy and producing a strongly adhering coating.

When dealing with electrocodeposition for a MMC, understanding the particle stability in the colloidal electroplating bath is crucial because the properties of the resulting composites change significantly with the preferential embedding of individual particles [39]. The particle size and zeta potential (Table 2) of the Cu-Ni plating solutions were measured to examine the stability of the dispersion of the Mt platelets in the electroplating bath. In an aqueous solution, the Mt size ranged from 430 to 525 nm. As the Mt is introduced into the plating solution, the particle size significantly increases versus the aqueous solution and continues to rise with increased amounts of Mt added to the plating bath. This change is probably due the adsorption of Cu and Ni ions onto the surface of the negatively charged platelets causing some platelet agglomeration. The Mt concentration (0.05–0.15%) in an aqueous solution produced zeta potential values of approximately −40 mV, indicating the exfoliated Mt platelets yield a stable dispersion in an aqueous solution. Typically, an ideal zeta potential for nanoparticle dispersion would be greater than ±25 mV. The Cu-Ni solution incorporated with the Mt platelets produced zeta potential values of approximately −20 mV, which are less stable than the Mt only solution. Adsorption of Cu and Ni onto the interface of the Mt platelet causes the zeta potential value to move towards a more positive value, which leads to small decrease in the electrostatic stabilization of the dispersion into the Cu-Ni plating bath. Although the dispersion of the Mt in the plating solution was slightly unstable, the dispersion was stable long enough for the deposition time to produce the composite coatings without having to be mechanically stirred. A specialty designed inverted cell was used for the deposition of the MMC coatings along with convection of the solution using nitrogen gas; this aided incorporation of the platelets into the coating through a combination of dispersion stability, slight gravity, and complexation with the cations in the plating solution.

3.3. Film Thickness. The film thickness of the pure 90-10 Cu-Ni and 90-10 Cu-Ni-Mt coatings was measured by profilometry to determine if the incorporation of Mt affected the coating thickness (Table 3). All of the coatings were electrochemically deposited up to 30 Coulombs of charge. The Mt had no effect on the current efficiency of the electrodeposition process as the thickness of the coatings did not decrease with incorporation of Mt. However, the coatings did get slightly thicker as the Mt percentage increased, which is probably due to the incorporation of the Mt into the metal matrix corresponding to a slight increase in surface roughness.

Table 3: Film thickness measured by a profilometer of the pure 90-10 Cu-Ni and Cu-Ni-Mt composite coatings deposited to 30 Coulombs of charge. Crystallite sizes of the pure 90-10 Cu-Ni and Cu-Ni-Mt composite coatings calculated from the Scherrer equation using X-ray diffraction data.

Coatings	Film thickness (μm) ($n = 3$)	Crystallite size (nm) ($n = 3$)
Cu-Ni	6.12 ± 0.04	58 ± 5
Cu-Ni-0.05% Mt	6.17 ± 0.03	19 ± 3
Cu-Ni-0.10% Mt	6.20 ± 0.05	16 ± 4
Cu-Ni-0.15% Mt	6.24 ± 0.07	12 ± 3

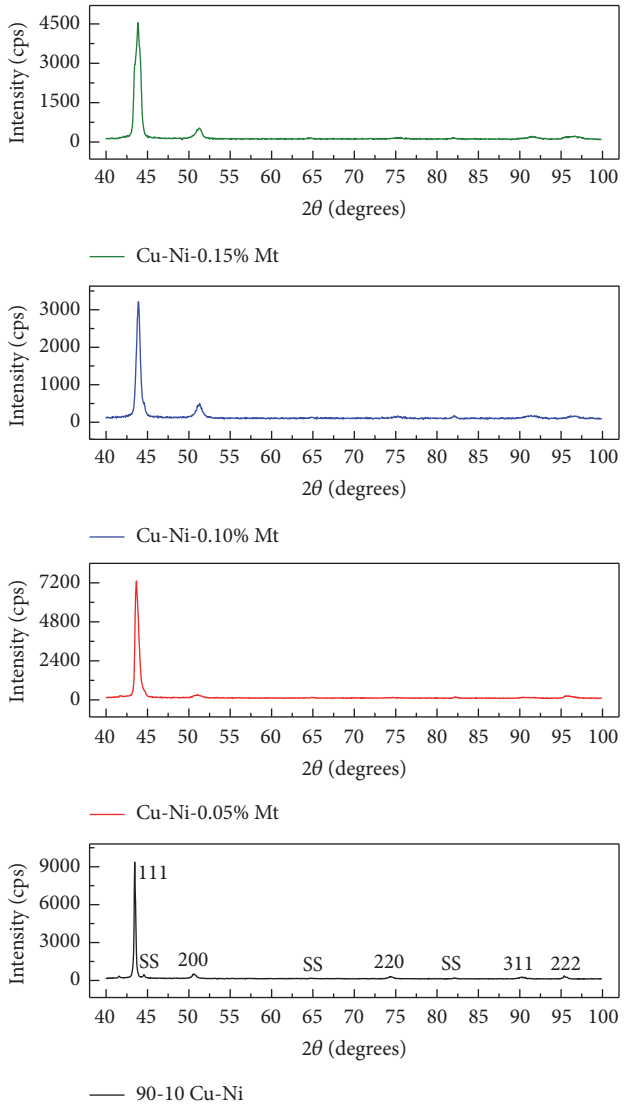

Figure 3: X-ray diffraction patterns of 90-10 Cu-Ni and Cu-Ni-Mt nanocomposite coatings run from 40–100° 2θ at a step size of 0.05° and dwell time of 1 sec (ss: steel substrate).

3.4. X-Ray Diffraction and Scanning Electron Microscopy. The X-ray diffraction (XRD) scans (shown in Figure 3) for the Cu-Ni alloy and Cu-Ni-Mt composite coatings were performed to analyze the crystal structure and measure the crystallite size. All of the XRD patterns show typical fcc reflections corresponding to the (111) crystallographic plane of Cu-Ni, as seen in Figure 3. Note that the reflections corresponding to the reinforced Mt nanoparticles for the composite coatings are not seen in the XRD patterns even at low 2θ angles due to complete exfoliation of Mt.

For the Cu-Ni alloy, only one peak is present for each reflection because the Cu-Ni alloy is an isomorphous binary alloy, which means the two metals are completely soluble in each other and have one type of crystal structure (fcc) with little to no strain [49]. The (111) major reflection at 43.51° is shifted between the values of pure copper at 43.297° (PDF # 00-004-0836) and pure nickel at 44.508° (PDF # 00-004-0850). The (111) reflection starts to broaden with the addition of Mt, as seen in Figure 3, which indicates a decrease in the crystallite size of the composite coatings. The crystallite size for each film was calculated using the Scherrer equation:

$$B_r = \frac{k\lambda}{L\cos\theta}. \quad (1)$$

The Gaussian peak fit method of $B_r^2 = B_o^2 - B_i^2$ was used as part of the calculation, where B_o is the peak broadening for the coating and B_i is the instrumental broadening calculated using a silicon standard. The proportionality constant k was assumed to be 1, λ = 0.15406 nm from the Cu Kα radiation, and θ is the position of the (111) reflection. The calculated crystallite sizes are listed in Table 3 and indicate that the crystallite size continues to decrease in the nanometer range as the amount of Mt increases in the coatings. Other researchers have reported similar decrease in crystallite size with addition of nanoparticles for electrodeposited coatings. The presence of the nanoparticles provides nucleation sites enhancing the nucleation process while inhibiting crystal growth; thus the presence of Mt may lead to structural refinement [50–53].

The surface morphology of the pure Cu-Ni alloy and Cu-Ni-Mt composite coatings is shown in Figure 4. All the films have very compact, uniform coverage across the substrate. With the incorporation of the Mt into the Cu-Ni matrix, the platelets are visible in the coatings (some are outlined in red) and are embedded into the coating.

3.5. Atomic Absorption Spectroscopy and Energy Dispersion Spectroscopy. Atomic absorption spectroscopy (AAS) was performed to determine the composition of the Cu-Ni coatings. The AAS analysis showed that the composition of the 90-10 Cu-Ni electrodeposited coatings was 88 ± 1% for copper and 12 ± 1% for nickel. EDS was also performed to evaluate the Cu, Ni, Si, and Al surface composition of the coatings. The Si and Al were measured since these are

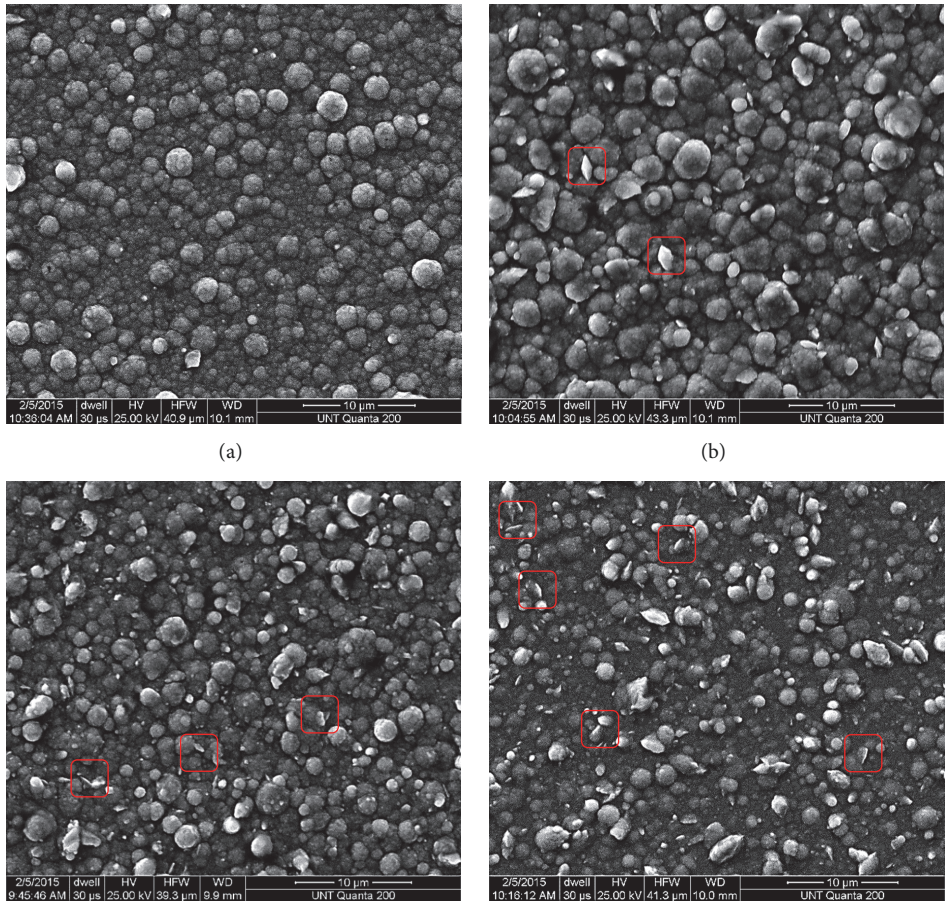

Figure 4: SEM surface micrographs of (a) 90-10 Cu-Ni, (b) 90-10 Cu-Ni-0.05% Mt, (c) 90-10 Cu-Ni-0.10% Mt, and (d) 90-10 Cu-Ni-0.15% Mt. Scale is 10 μm. Red squares show examples of Mt platelets.

Table 4: Energy dispersion spectroscopy data of the pure 90-10 Cu-Ni and Cu-Ni-Mt composite coatings.

Coatings	Copper (%)	Nickel (%)	Silicon (%)	Aluminum (%)
Cu-Ni	89.65	10.35	---	---
Cu-Ni-0.05% Mt	86.05	11.50	1.49	0.96
Cu-Ni-0.10% Mt	84.90	11.32	2.35	1.43
Cu-Ni-0.15% Mt	83.97	11.21	2.94	1.88

major elemental components in the Mt structure. The EDS results are presented in Table 4 and show that the Si and Al content increased as the amount of Mt added to the plating solution also increased, which confirms the incorporation of the Mt platelets in the coatings. XPS depth profile analysis also showed presence of silicon and aluminum throughout the coatings.

As the Mt incorporation increased, the Cu and Ni percentages changed slightly in the coatings. With addition of Mt to the plating bath, the nickel percentage slightly increased while the copper decreased from ~90 to 84%. Previous data has shown that Ni ions adsorb to the surface of the Mt platelet [42]. Nickel is in excess in the solution because of the deposition conditions and most of the copper is complexed with citrate [44]. At pH values greater than 5, the heterobinuclear deprotonated species, $CuNiCit_2H_2^{4-}$, predominate in the solution over the binary deprotonated species, $Cu_2Cit_2H_2^{4-}$. With Cu present in the plating solution, less citrate is available to complex with the nickel, resulting in a lower concentration of the certain species containing nickel and citrate ($NiCit_2H^{3-}$ and $NiCit_2^{4-}$) and an increase in $NiCit^-$ species [44]. The slight change in the Cu-Ni ratio of the coatings can be attributed to the embedding of the Mt particles with a greater percentage of Ni over Cu adsorbed onto the surface of the platelets.

3.6. Hardness and Shear Strength. There are two factors that play a major role in the hardness of the MMC coating: the amount of particles embedded into the matrix and the microstructure of the metallic matrix. The microstructure of

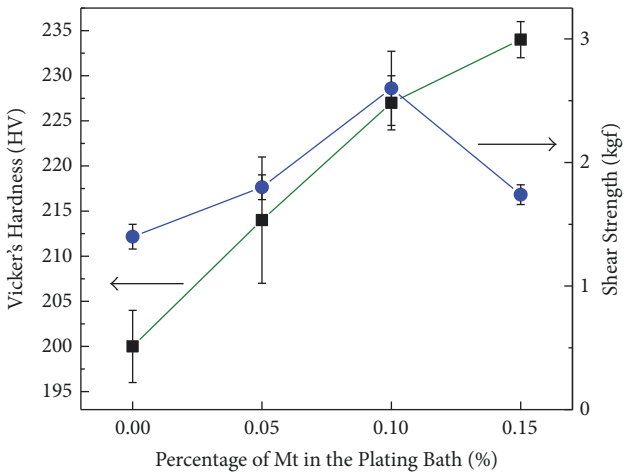

Figure 5: Microhardness data for 90-10 Cu-Ni and Cu-Ni-Mt nanocomposite coatings versus the percentage of Mt in the plating solution (left axis). The shear adhesion strength of pure 90-10 Cu-Ni and Cu-Ni-Mt composite coatings versus the percentage of Mt in the plating solution (right axis).

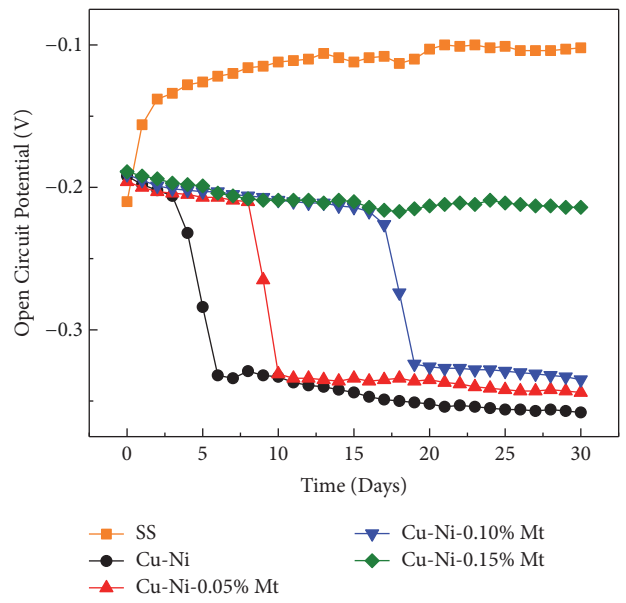

Figure 6: Plot of the immersion test for the 90-10 Cu-Ni and Cu-Ni-Mt nanocomposite coatings measured by OCP versus time for 30 days in Burkholder's Formula B solution.

the metallic matrix is controlled by the parameters of the electrodeposition process including bath concentration of the ions, pH, applied potential, and the current density [46, 54]. The amount of the particles embedded into the matrix is in direct relation to the bath concentration, size of particles, solution pH, and type of reinforcement material. Mt has shown the ability to increase the hardness substantially in a pure nickel matrix [37]. The effect of embedding Mt platelets into the Cu-Ni matrix on the microhardness was analyzed and the results are shown in Figure 5. The microhardness of the Cu-Ni coatings increases by 17% with the incorporation of 0.15% Mt into the Cu-Ni matrix. Since all the coatings have a nanocrystalline Cu-Ni matrix, the increasing hardness of the Cu-Ni-Mt composite coatings with increasing Mt content seems primarily to be due to the enhanced dispersion strengthening effects. In addition, the presence of the finer grains helps to impede the dislocation motion resulting in an increase in the microhardness [55]. Therefore, the increase in hardness for the Cu-Ni-Mt coatings can also be attributed to grain refining which is related to the nucleation of small grains on the surface of the incorporated particles, which leads to an overall structural refinement also seen in the XRD data. Alternatively, the hard Mt nanoparticles dispersed within the Cu-Ni matrix could enhance the resistance to localized deformation of the matrix leading to the sharp increase in the hardness of the composites, especially at 0.15% Mt addition.

The measured adhesion strength for the coatings is also shown in Figure 5. The adhesion strength of all the nanocomposite coatings exceeds that of the Cu-Ni matrix alone. The presence of the nanoplatelets provides enhanced resistance to the knife movement. An 85% increase was observed for the 0.10% Mt. At this lower level of Mt particles in the Cu-Ni matrix, reinforcement in the composite improved the bonding, which can be attributed to both the mechanical load transfer from the matrix to the Mts and the high specific surface area of this material. However, the shear adhesion strength began to decrease beyond 0.10% Mt since an increase in number of platelets in the coating allows more substrate-platelet contact and decreases the effective area of the matrix-substrate contact.

3.7. Immersion Study. An immersion test of open circuit potential (OCP) versus time was performed to evaluate the stability of the Cu-Ni coating incorporated with and without Mt particles (Figure 6). The OCP of pure Cu-Ni, Cu-Ni-0.05% Mt, and Cu-Ni-0.10% Mt films was shifted cathodically after three, eight, and seventeen days, respectively. The OCP of Cu-Ni-0.15% Mt stayed stable over the extended period of 30 days compared to the other coatings. Eventually, this coating's OCP value also shifted cathodically after 38 days, which indicates the same Cu_2O protective layer formation. Al-Muhanna and Habib also observed a cathodic shift in OCP for Cu-Ni in the first 10–15 days of their study leading to lower corrosion resistance. This is due to the period of time it takes to form the protective oxide layers [56]. The study also showed that the temperature of the seawater influences the corrosion resistance, where seawater temperature changes caused the OCP to oscillate over time. The result of the immersion test indicates that Mt provides a barrier protection for the Cu-Ni matrix, which stabilizes and increases the corrosion resistance.

3.8. Potentiodynamic Polarization. The corrosion resistance of Cu-Ni and Cu-Ni-Mt composite coatings was evaluated using potentiodynamic polarization and shown in Figure 7. The corrosion values were measured after immersing the prepared coatings for 30 days in Burkholder's Formula B simulated seawater at 25°C. Table 5 lists the corrosion results

Table 5: E_{corr}, i_{corr}, and polarization resistance (R_p) of the pure 90-10 Cu-Ni and Cu-Ni-Mt composite coatings.

Coatings	E_{corr} (V)	i_{corr} (A)	R_p (kΩ·cm^2)
Cu-Ni	−0.349	2.50×10^{-6}	11.77
Cu-Ni-0.05% Mt	−0.347	1.66×10^{-6}	15.50
Cu-Ni-0.10% Mt	−0.336	1.56×10^{-6}	17.10
Cu-Ni-0.15% Mt	−0.220	9.84×10^{-7}	33.28

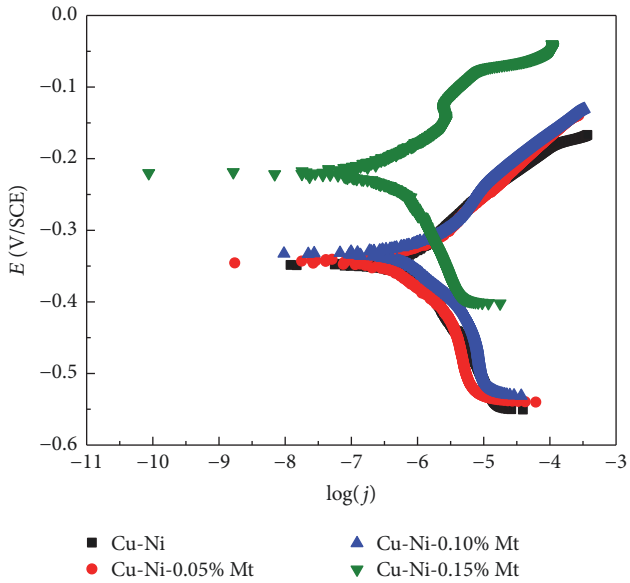

Figure 7: Potentiodynamic polarization plots for the 90-10 Cu-Ni and Cu-Ni-Mt nanocomposite coatings after being immersed in Burkholder's Formula B solution for 30 days.

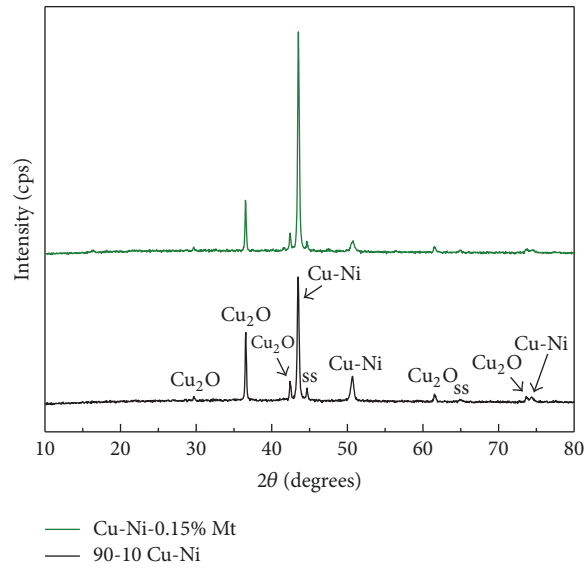

Figure 8: X-ray diffraction scans of the 90-10 Cu-Ni and Cu-Ni-0.15% Mt coatings after soaking in the simulated seawater for 30 days to determine the corrosion products (ss: steel substrate).

for the measurement. The E_{corr} value for the Cu-Ni-0.15% Mt is more noble than the other coatings which was evident in the immersion study because of the increased stability provided by the Mt platelets in the Cu-Ni matrix. With an increase of concentration of Mt into the Cu-Ni coatings, the i_{corr} values decreased from 2.50×10^{-6} to 9.84×10^{-7} A/cm^2. Varea et al. also noted a similar i_{corr} value for electroplated 90-10 Cu-Ni at 1.8×10^{-6} A/cm^2 [48]. The R_p value of the pure Cu-Ni coating was 11.77 kΩ·cm^2, whereas the Cu-Ni-0.15% Mt increased to 33.28 kΩ·cm^2. The addition of Mt into the Cu-Ni deposition process significantly increased the resistance to corrosion by providing barrier protection to slow the mean free path of corrosion. In addition, the embedded platelets at the surface decrease the exposed metallic area that could undergo corrosion attack and thus improve the corrosion resistance of the coatings. Each mechanism may play some role in the overall corrosion protection of the coatings. These types of mechanism have been proposed for other electrodeposited composite coatings such as Ni-Co/SiC [57] and Zn-TiO_2 [58, 59] as well as Ni-Fe composite coatings [60].

An oxide layer of Cu_2O has been confirmed to form for Cu-Ni alloys exposed to chloride environments [30]. During the corrosion of copper alloys, copper dissolution eventually creates $CuCl_2^-$ species which form cuprous oxide as the local pH at the interfaces increases [30, 33, 61]:

$$2CuCl_2^- + H_2O \longrightarrow Cu_2O + 2H^+ + 4Cl^- \quad (2)$$

The OCP studies show that the pure Cu-Ni coatings begin to form an oxide layer earliest, while the Cu-Ni-Mt coatings begin the oxide layer formation in order of Mt content, and the oxide layer becomes more porous with time. The presence of this passivating layer is confirmed by X-ray diffraction. Figure 8 is the XRD scans run from 10–80° for the pure 90-10 Cu-Ni and Cu-Ni-0.15% Mt coatings, after soaking for 30 days in the simulated seawater. The presence of the main constituent for corrosion protection, Cu_2O, was identified for both pure Cu-Ni and Cu-Ni-0.15% Mt (as well as the Cu-Ni-0.05% Mt and Cu-Ni-0.10% Mt samples). Ma et al. also showed X-ray diffraction reflections for Cu_2O in the corrosion products of a 90-10 Cu-Ni sample left in natural seawater [32]. When the concentration of nickel is below 40%, an outer layer of $Cu_2(OH)_3Cl$ and a dense inner layer of Cu_2O have been shown to be the passivating layers in high chloride environments [30]. Cu_2O is known to be the main constituent for good corrosion resistance because of its low electronic conductivity. The cuprous oxide layer forms first and once the Cu_2O layer has formed, a $Cu_2(OH)_3Cl$

layer is produced by precipitation from the dissolution of Cu^{2+} ions [30, 32]. For the electrodeposited coatings, the X-ray diffraction data indicates that, for the 30-day time period, Cu_2O begins formation on the surface of the coatings.

As noted earlier, the R_p values obtained from linear polarization increase as the Mt amount increases, compared to the pure Cu-Ni coating. The corrosion resistance improves as the Mt content in the Cu-Ni matrix increases which is consistent with the incorporation of Mt nanoplatelets providing an additional barrier and a formation of a passive Cu_2O layer. The Mt particles act as inert physical barriers to the initiation and development of defect corrosion, modifying the microstructure of the Cu-Ni film and hence improving the corrosion resistance of the coating.

4. Conclusions

The composition of the Cu-Ni coating was controlled by the bath conditions and the applied voltage to produce a 90-10 ratio. Incorporation of exfoliated Mt nanoplatelets into the Cu-Ni matrix by electrodeposition improved both the corrosion resistance and mechanical properties. The 0.15% Mt addition produced the best increase in the hardness and the corrosion resistance, whereas the 0.10% Mt addition provided the best shear adhesion strength. Also, the 0.15% Mt addition helped to stabilize the corrosion potential during the 30-day immersion study in simulated seawater. The results indicate that the enhancement in the corrosion protection is due to the grain refinement and barrier protection provided by the addition of the Mt nanoplatelets to the coatings.

Data Availability

The data used to support the findings of this study are available from the corresponding author upon request.

Disclosure

The statements made herein are solely the responsibility of the authors.

Conflicts of Interest

The authors declare that there are no conflicts of interest regarding the publication of this paper.

Acknowledgments

This work was made possible by NPRP Grant 4-306-2-111 from the Qatar National Research Fund (a Member of The Qatar Foundation). The authors thank Stephen Sanders for help with instrumentation. The authors also acknowledge the Center for Advanced Research and Technology (CART) and the Advanced Materials and Manufacturing Processes Institute (AMMPI) at the University of North Texas.

References

[1] I. A. W. Ma, A. Sh, K. Ramesh, B. Vengadaesvaran, S. Ramesh, and A. K. Arof, "Anticorrosion properties of epoxy-nanochitosan nanocomposite coating," *Progress in Organic Coatings*, vol. 113, pp. 74–81, 2017.

[2] K. A. Zahidah, S. Kakooei, M. C. Ismail, and P. Bothi Raja, "Halloysite nanotubes as nanocontainer for smart coating application: A review," *Progress in Organic Coatings*, vol. 111, pp. 175–185, 2017.

[3] H. Wang, Z-H. Zhang, Z-Y. Hu et al., "Improvement of interfacial interaction and mechanical properties in copper matrix composites reinforced with copper coated carbon nanotubes," *Materials Science and Engineering: A*, vol. 715, pp. 163–173, 2018.

[4] S. Ramalingam, V. S. Muralidharan, and A. Subramania, "Electrodeposition and characterization of Cu-TiO_2 nanocomposite coatings," *Journal of Solid State Electrochemistry*, vol. 13, no. 11, pp. 1777–1783, 2009.

[5] F. C. Walsh and C. Ponce de Leon, "A review of the electrodeposition of metal matrix composite coatings by inclusion of particles in a metal layer: an established and diversifying technology," *Transactions of the IMF*, vol. 92, no. 2, pp. 83–98, 2014.

[6] I. Zamblau, S. Varvara, and L. M. Muresan, "Corrosion behavior of Cu-SiO_2 nanocomposite coatings obtained by electrodeposition in the presence of cetyl trimethyl ammonium bromide," *Journal of Materials Science*, vol. 46, no. 20, pp. 6484–6490, 2011.

[7] S. Dehgahi, R. Amini, and M. Alizadeh, "Microstructure and corrosion resistance of Ni-Al_2O_3-SiC nanocomposite coatings produced by electrodeposition technique," *Journal of Alloys and Compounds*, vol. 692, pp. 622–628, 2017.

[8] M. Rosso, "Ceramic and metal matrix composites: Route and properties," *Journal of Materials Processing Technology*, vol. 175, pp. 364–375, 2006.

[9] B. Reddy, "Electrodeposition of metal matrix nanocomposites: Improvement of the chemical characterization techniques," in *Advances in Nanocomposites - Synthesis, Characterization and Industrial Applications*, pp. 503–526, InTech, 2011 (Chapter 21).

[10] M. Musiani, "Electrodeposition of composites: An expanding subject in electrochemical materials science," *Electrochimica Acta*, vol. 45, no. 20, pp. 3397–3402, 2000.

[11] T. V. Sviridova, A. S. Logvinovich, and D. V. Sviridov, "Electrochemical growing of Ni-MoO_3 nanocomposite coatings via redox mechanism," *Surface and Coatings Technology*, vol. 319, pp. 6–11, 2017.

[12] C. T. J. Low, R. G. A. Wills, and F. C. Walsh, "Electrodeposition of composite coatings containing nanoparticles in a metal deposit," *Surface and Coatings Technology*, vol. 201, no. 1-2, pp. 371–383, 2006.

[13] A. K. Chaudhari and V. B. Singh, "Studies on Electrodeposition, Microstructure and Physical Properties of Ni-Fe/In_2O_3 Nanocomposite," *Journal of The Electrochemical Society*, vol. 162, no. 8, pp. D341–D349, 2015.

[14] L. Shi, C. Sun, P. Gao, F. Zhou, and W. Liu, "Mechanical properties and wear and corrosion resistance of electrodeposited Ni-Co/SiC nanocomposite coating," *Applied Surface Science*, vol. 252, no. 10, pp. 3591–3599, 2006.

[15] B. Bakhit, A. Akbari, F. Nasirpouri, and M. G. Hosseini, "Corrosion resistance of Ni-Co alloy and Ni-Co/SiC nanocomposite coatings electrodeposited by sediment codeposition technique," *Applied Surface Science*, vol. 307, pp. 351–359, 2014.

[16] H.-Y. Zheng and M.-Z. An, "Electrodeposition of Zn-Ni-Al_2O_3 nanocomposite coatings under ultrasound conditions," *Journal of Alloys and Compounds*, vol. 459, no. 1-2, pp. 548–552, 2008.

[17] K. Arunsunai Kumar, G. Paruthimal Kalaignan, and V. S. Muralidharan, "Direct and pulse current electrodeposition of Ni-W-TiO_2 nanocomposite coatings," *Ceramics International*, vol. 39, no. 3, pp. 2827–2834, 2013.

[18] V. Torabinejad, M. Aliofkhazraei, A. S. Rouhaghdam, M. H. Allahyarzadeh, T. Kasama, and H. Alimadadi, "Mechanical properties of multilayer Ni-Fe and Ni-Fe-Al_2O_3 nanocomposite coating," *Materials Science and Engineering: A Structural Materials: Properties, Microstructure and Processing*, vol. 700, pp. 448–456, 2017.

[19] V. Torabinejad, M. Aliofkhazraei, A. S. Rouhaghdam, and M. H. Allahyarzadeh, "Tribological performance of Ni-Fe-Al_2O_3 multilayer coatings deposited by pulse electrodeposition," *Wear*, vol. 380-381, pp. 115–125, 2017.

[20] V. Torabinejad, A. S. Rouhaghdam, M. Aliofkhazraei, and M. H. Allahyarzadeh, "Electrodeposition of Ni-Fe and Ni-Fe-(nano Al_2O_3) multilayer coatings," *Journal of Alloys and Compounds*, vol. 657, pp. 526–536, 2016.

[21] M. H. Allahyarzadeh, M. Aliofkhazraei, A. R. S. Rouhaghdam, and V. Torabinejad, "Electrodeposition of Ni-W-Al_2O_3 nanocomposite coating with functionally graded microstructure," *Journal of Alloys and Compounds*, vol. 666, pp. 217–226, 2016.

[22] M. H. Allahyarzadeh, M. Aliofkhazraei, A. R. S. Rouhaghdam, and V. Torabinejad, "Electrochemical tailoring of ternary Ni-W-Co(Al_2O_3) nanocomposite using pulse reverse technique," *Journal of Alloys and Compounds*, vol. 705, pp. 788–800, 2017.

[23] B. E. Torres Bautista, M. L. Carvalho, A. Seyeux et al., "Effect of protein adsorption on the corrosion behavior of 70Cu-30Ni alloy in artificial seawater," *Bioelectrochemistry*, vol. 97, pp. 34–42, 2014.

[24] S. J. Yuan and S. O. Pehkonen, "Surface characterization and corrosion behavior of 70/30 Cu-Ni alloy in pristine and sulfide-containing simulated seawater," *Corrosion Science*, vol. 49, no. 3, pp. 1276–1304, 2007.

[25] X. Zhu and T. Lei, "Characteristics and formation of corrosion product films of 70Cu-30Ni alloy in seawater," *Corrosion Science*, vol. 44, no. 1, pp. 67–79, 2002.

[26] R. Francis, "The corrosion of copper and its alloys – A practical guide for engineers, Chapter on Corrosion in Waters," *343-348, NACE International*, pp. 343–348, 2009.

[27] A. M. Helal, A. Al-Jafri, and A. Al-Yafeai, "Enhancement of existing MSF plant productivity through design modification and change of operating conditions," *Desalination*, vol. 307, pp. 76–86, 2012.

[28] W. Schleich, "Typical failures of cuni 90/10 seawater tubing systems and how to avoid them," *Eurocorr*, pp. 1–10, 2004.

[29] W. Schleich, R. Feser, G. Schmitt, S. Haarmann, and K. Schnier, "Effect of seawater chlorination on the erosion corrosion behaviour of CuNi 90/10," *Eurocorr*, pp. 1–14, 2007.

[30] I. Milošev and M. Metikoš-Huković, "The behaviour of Cu-xNi (x = 10 to 40 wt%) alloys in alkaline solutions containing chloride ions," *Electrochimica Acta*, vol. 42, no. 10, pp. 1537–1548, 1997.

[31] B. V. Appa Rao, K. Chaitanya Kumar, and N. Y. Hebalkar, "X-ray photoelectron spectroscopy depth-profiling analysis of surface films formed on Cu-Ni (90/10) alloy in seawater in the absence and presence of 1,2,3-benzotriazole," *Thin Solid Films*, vol. 556, pp. 337–344, 2014.

[32] A. L. Ma, S. L. Jiang, Y. G. Zheng, and W. Ke, "Corrosion product film formed on the 90/10 copper-nickel tube in natural seawater: Composition/structure and formation mechanism," *Corrosion Science*, vol. 91, pp. 245–261, 2015.

[33] M. Metikos-Hukovic, I. Škugor, Z. Grubač, and R. Babić, "Complexities of corrosion behaviour of copper-nickel alloys under liquid impingement conditions in saline water," *Electrochimica Acta*, vol. 55, no. 9, pp. 3123–3129, 2010.

[34] D. Bian, T. V. Aradhyula, Y. Guo, and Y. Zhao, "Improving tribological performance of chemically bonded phosphate ceramic coatings reinforced by graphene nano-platelets," *Ceramics International*, vol. 43, no. 15, pp. 12466–12471, 2017.

[35] A. Q. Wang and T. D. Golden, "Electrochemical Formation of Cerium Oxide/Layered Silicate Nanocomposite Films," *Journal of Nanotechnology*, vol. 2016, Article ID 8459374, 7 pages, 2016.

[36] Y. H. Ahmad, J. Tientong, N. D'Souza, T. D. Golden, and A. M. A. Mohamed, "Salt water corrosion resistance of electrodeposited Ni-layered silicate nanocomposite coatings from Watts' type solution," *Surface and Coatings Technology*, vol. 242, pp. 170–176, 2014.

[37] J. Tientong, Y. H. Ahmad, M. Nar, N. D'souza, A. M. A. Mohamed, and T. D. Golden, "Improved mechanical and corrosion properties of nickel composite coatings by incorporation of layered silicates," *Materials Chemistry and Physics*, vol. 145, no. 1-2, pp. 44–50, 2014.

[38] X. Cui, W. Wei, H. Liu, and W. Chen, "Electrochemical study of codeposition of Al particle-Nanocrystalline Ni/Cu composite coatings," *Electrochimica Acta*, vol. 54, no. 2, pp. 415–420, 2008.

[39] M. Hashemi, S. Mirdamadi, and H. R. Rezaie, "Effect of SiC nanoparticles on microstructure and wear behavior of Cu-Ni-W nanocrystalline coating," *Electrochimica Acta*, vol. 138, pp. 224–231, 2014.

[40] A. Panda and E. J. Podlaha, "Nanoparticles to Improve Mass Transport Inside Deep Recesses," *Electrochemical and Solid-State Letters*, vol. 6, no. 11, pp. C149–C152, 2003.

[41] C. R. Thurber, Y. H. Ahmad, S. F. Sanders et al., "Electrodeposition of 70-30 Cu-Ni nanocomposite coatings for enhanced mechanical and corrosion properties," *Current Applied Physics*, vol. 16, no. 3, pp. 387–396, 2016.

[42] R. A. Horch, T. D. Golden, N. A. D'Souza, and L. Riester, "Electrodeposition of nickel/montmorillonite layered silicate nanocomposite thin films," *Chemistry of Materials*, vol. 14, no. 8, pp. 3531–3538, 2002.

[43] E. J. Podlaha, Ch. Bonhote, and D. Landolt, "Mathematical model and experimental study of the electrodeposition of Ni-Cu alloys from complexing electrolytes," *Electrochimica Acta*, vol. 39, no. 18, pp. 2649–2657, 1994.

[44] T. A. Green, A. E. Russell, and S. Roy, "The development of a stable citrate electrolyte for the electrodeposition of copper-nickel alloys," *Journal of The Electrochemical Society*, vol. 145, no. 3, pp. 875–881, 1998.

[45] S. Rode, C. Henninot, and M. Matlosz, "Complexation chemistry in nickel and copper-nickel alloy plating from citrate baths," *Journal of The Electrochemical Society*, vol. 152, no. 4, pp. C248–C254, 2005.

[46] J. Tientong, C. R. Thurber, N. D'Souza, A. Mohamed, and T. D. Golden, "Influence of Bath Composition at Acidic pH on Electrodeposition of Nickel-Layered Silicate Nanocomposites for Corrosion Protection," *International Journal of Electrochemistry*, vol. 2013, pp. 1–8, 2013.

[47] J. P. Bidwell and S. Spotte, *Simulated seawaters: Formulas and methods*, Jones and Bartlett Publishers, Boston, USA, 1985.

[48] A. Varea, E. Pellicer, S. Pané et al., "Mechanical properties and corrosion behaviour of nanostructured Cu-rich CuNi electrodeposited films," *International Journal of Electrochemical Science*, vol. 7, no. 2, pp. 1288–1302, 2012.

[49] M. Alper, H. Kockar, M. Safak, and M. C. Baykul, "Comparison of Ni-Cu alloy films electrodeposited at low and high pH levels," *Journal of Alloys and Compounds*, vol. 453, no. 1-2, pp. 15–19, 2008.

[50] M. H. Allahyarzadeh, M. Aliofkhazraei, A. R. S. Rouhaghdam, and V. Torabinejad, "Structure and wettability of pulsed electrodeposited Ni-W-Cu-(α-alumina) nanocomposite," *Surface and Coatings Technology*, vol. 307, pp. 525–533, 2016.

[51] Y. Yang and Y. F. Cheng, "Fabrication of Ni-Co-SiC composite coatings by pulse electrodeposition - Effects of duty cycle and pulse frequency," *Surface and Coatings Technology*, vol. 216, pp. 282–288, 2013.

[52] S. R. Allahkaram, S. Golroh, and M. Mohammadalipour, "Properties of Al_2O_3 nano-particle reinforced copper matrix composite coatings prepared by pulse and direct current electroplating," *Materials and Corrosion*, vol. 32, no. 8-9, pp. 4478–4484, 2011.

[53] I. Gurrappa and L. Binder, "Electrodeposition of nanostructured coatings and their characterization—a review," *Science and Technology of Advanced Materials*, vol. 9, no. 4, Article ID 043001, 2008.

[54] E. B. Budevski, G. T. Staikov, and W. J. Lorenz, *Electrochemical phase formation and growth, An introduction to the initial stages of metal deposition*, ISBN 978-3-527-61492-9, Wiley-VCH, Weinheim, Germany, 1996.

[55] H. Gül, F. Kiliç, S. Aslan, A. Alp, and H. Akbulut, "Characteristics of electro-co-deposited Ni-Al_2O_3 nano-particle reinforced metal matrix composite (MMC) coatings," *Wear*, vol. 267, no. 5-8, pp. 976–990, 2009.

[56] K. Al-Muhanna and K. Habib, "Corrosion behavior of different alloys exposed to continuous flowing seawater by electrochemical impedance spectroscopy (EIS)," *Desalination*, vol. 250, no. 1, pp. 404–407, 2010.

[57] B. Bakhit and A. Akbari, "Effect of particle size and co-deposition technique on hardness and corrosion properties of Ni-Co/SiC composite coatings," *Surface and Coatings Technology*, vol. 206, no. 23, pp. 4964–4975, 2012.

[58] M. Sajjadnejad, M. Ghorbani, and A. Afshar, "Microstructure-corrosion resistance relationship of Direct and Pulse Current electrodeposited Zn-TiO_2 nanocomposite coatings," *Ceramics International*, vol. 41, no. 1, pp. 217–224, 2014.

[59] B. M. Praveen and T. V. Venkatesha, "Electrodeposition and properties of Zn-nanosized TiO_2 composite coatings," *Applied Surface Science*, vol. 254, no. 8, pp. 2418–2424, 2008.

[60] V. Torabinejad, M. Aliofkhazraei, S. Assareh, M. H. Allahyarzadeh, and A. S. Rouhaghdam, "Electrodeposition of Ni-Fe alloys, composites, and nano coatings–A review," *Journal of Alloys and Compounds*, vol. 691, pp. 841–859, 2017.

[61] S. Colin, E. Beche, R. Berjoan, H. Jolibois, and A. Chambaudet, "An XPS and AES study of the free corrosion of Cu-, Ni- and Zn-based alloys in synthetic sweat," *Corrosion Science*, vol. 41, no. 6, pp. 1051–1065, 1999.